Conf-911179--2

2

PNL-SA--20244

DE92 004509

SENSITIZATION AND IGSCC SUSCEPTIBILITY PREDICTION IN STAINLESS STEEL PIPE WELDMENTS

D. G. Atteridge S. M. Bruemmer
J. W. Simmons Ming Li

November 1991

Presented at the
Life Prediction of Corrodible
Structures Conference
November 5-8, 1991
Hawaii

Work supported by
the U.S. Department of Energy
under Contract DE-AC06-76RLO 1830

Pacific Northwest Laboratory
Richland, Washington 99352

DISCLAIMER

Sensitization and IGSCC Susceptibility Prediction in Stainless Steel Pipe Weldments

David G. Atteridge
Oregon Graduate Institute of Science and Technology
19600 NW von Neumann Drive
Beaverton, OR 97006-1999

Stephen M. Bruemmer
Pacific Northwest Laboratory
Richland, WA 99352

John W. Simmons
Oregon Graduate Institute of Science and Technology
19600 NW von Neumann Drive
Beaverton, OR 97006-1999

Ming Li
Oregon Graduate Institute of Science and Technology
19600 NW von Neumann Drive
Beaverton, OR 97006-1999

Abstract

An analytical model, based on prediction of chromium depletion, has been developed for predicting thermomechanical effects on austenitic stainless steel intergranular stress corrosion cracking (IGSCC) susceptibility. Model development and validation is based on sensitization development analysis of over 30 Type 316 and 304 stainless steel heats. The data base included analysis of deformation effects on resultant sensitization development. Continuous Cooling sensitization behavior is examined and modelled with and without strain. Gas tungsten arc (GTA) girth pipe weldments are also characterized by experimental measurements of heat affected zone (HAZ) temperatures, strains and sensitization during/after each pass; pass by pass thermal histories are also predicted. The model is then used to assess pipe chemistry changes on IGSCC resistance.

Introduction

It has long been known that IGSCC of austenitic Type 300 Series stainless steels (SS) is directly related to the presence of grain boundary chromium depletion, and that this depletion, also called "sensitization", is caused by the formation of grain boundary

chromium carbides/nitrides.[1] Thus it is well documented that susceptibility to IGSCC is caused by a diffusion controlled process. However, quantification of this phenomena is still an active research area, and the research reported herein pertains to the development of a computer-based model capable of predicting IGSCC susceptibility in the heat affected zone (HAZ) of Type 304 and 316 SS girth pipe weldments.

Model predictions are based on prediction of chromium depletion at grain boundaries. It is assumed that as grain boundary sensitization increases susceptibility to IGSCC increases. A demonstration of this relationship determined by constant extension rate (CERT) testing is presented in Figure 1.[1,2] Note that "EPR-DOS" is a measurement of degree of sensitization (DOS), as discussed in the Sensitization Measurement Section below. The model predicts levels of sensitization, with susceptibility to IGSCC estimated on a system by system assessment.

The model, SSDOS, originally developed by Bruemmer, assesses the effect of both thermodynamics and kinetics on the development of sensitization, as illustrated in Figure 2.[2,3] Thermodynamics are needed to assess chromium minimums at the matrix-carbide interface as a function of SS composition and diffusion temperature, see Figure 3. These matrix-carbide "equilibrium" chromium concentrations are assumed to control, and indeed be equal to, grain boundary chromium concentrations. Bruemmer assumed this was a valid first approximation due to increased grain boundary diffusivity, in comparison to matrix diffusivity. The chromium minimum is then used in diffusion calculations in developing chromium depletion grain boundary profiles as a function of temperature and time.

Original model concepts assumed instantaneous attainment of equilibrium chromium minimum values and allowed sensitization to develop as a function of temperature and time.[2-4] Modifications to the SSDOS isothermal section incorporated a nucleation time incubation period prior to initiation of diffusional growth of the chromium depletion zone.[2,3] Research into sensitization development induced by continuous cooling also indicates that inclusion of nucleation times is critical for realistic predictions of sensitization development.[5] Both isothermal and continuous cooling research work has shown that plastic strain dramatically increases sensitization development.[2-6] Work reported herein discusses recent developments in modeling continuous cooling experimental results and application of these techniques to prediction of weld induced sensitization.

Sensitization Measurement

Sensitization modeling is based on diffusional concepts which allow prediction of grain boundary chromium depletion, as defined by a chromium minimum and chromium depletion profile as a function of distance away from the grain boundary. It is possible to experimentally measure the exact chromium depletion profile using the scanning transmission electron microscope (STEM) and this has been done for many specimens as

a function of heat treatment and composition.[2-4;7-9] However, STEM analysis techniques are not applicable to large test matrix analysis. Thus the majority of sensitization measurements were carried out using the electrochemical potentiokinetic reactivation (EPR) test. This test was specifically developed to detect and quantify the presence of chromium depletion regions.

The single scan EPR test was used throughout this research project, with the measured EPR degree of sensitization (DOS) being determined as the integrated area under the voltage current trace normalized by grain size.[10-12] A schematic illustration of increasing DOS with increasing corrosion current flow from previously passivated specimen surfaces is shown in Figure 4. An empirical correlation between measured STEM chromium depletion and EPR-DOS allowed model predictions of EPR-DOS from basic predictions of Chromium depletion.[2,3,7,9]

Continuous Cooling Model Development

SSDOS treated continuous cooling induced sensitization development as step-wise isothermal sensitization development.[4] Small isothermal steps (determined based on cooling rate) at average temperatures were used to calculate total sensitization development. Cumulative sensitization from previous steps was first determined. Then sensitization at the active step was determined from the known initial sensitization level and the time at the active isothermal step. This new sensitization value was then input as the initial sensitization level for the next isothermal step.

The time at the active isothermal temperature needed to achieve the initial cumulative sensitization value was back calculated and then added to the hold time at the active isothermal temperature to yield an "effective" hold time. A new cumulative sensitization value is then calculated from this effective total hold time at the given active isothermal temperature. The accelerating effect of plastic strain was taken into account by simply multiplying chromium diffusivity by an empirically derived factor proportional to total strain.[2-4]

Predictions of continuous cooling sensitization development were made using SSDOS and compared with actual continuous cooling data developed using a Gleeble, equipment specifically developed for thermomechanical cycle simulation. A typical Gleeble thermal cycle is presented in Figure 5. Specimens were tested as a function of maximum (peak) temperature reached and linear cooling rate, as well as a function of prior strain.[5,13] Prior strain was achieved by controlled tensile elongation in an Instron testing machine at room temperature prior to specimen insertion in the Gleeble.

The continuous cooling test matrix presented in Table 1 was performed on a high carbon Type 316 SS with the following composition (wt%): 0.067C, 16.81Cr, 11.21Ni, 2.20Mo, 1.46Mn, 0.28Si, 0.016P, 0.071N. Comparison between predicted and measured EPR-DOS indicated that SSDOS consistently over predicted sensitization development,

Figure 6a.[5] The probable cause is the assumption of instantaneous carbide precipitation and development of minimum chromium grain boundary levels.

A more accurate prediction of continuous cooling sensitization was obtained by insertion of a module to predict nucleation time. This module was developed based on the assumption that carbides must first nucleate at sufficient density on the grain boundary prior to that boundary reaching an "equilibrium" chromium minimum. Chromium depletion calculations are not initiated until this nucleation time is reached.

It is still assumed that this chromium minimum concentration is instantaneously arrive at over the complete boundary once initial nucleation takes place. A more realistic assumption would be that this minimum concentration is, at least initially, only effective a given distance from the carbide site, and that this effective distance is a function of time at temperature. In addition, boundary-to-boundary variation would also have to be accounted for.

Calculation of nucleation time is carried out in essentially the same step-wise manner as sensitization development using the Manning-Loring method.[2,3] A nucleation fraction, based on total isothermal nucleation time at the active isothermal step, is calculated for each isothermal time step; step fractions are summed until a nucleation fraction of one is reached. Nucleation is then assumed to be complete and chromium depletion calculations are initiated.

Improved predictions of continuous cooling sensitization was obtained with the modified model (SSDOS-II). Comparisons with experimental data, Figures 7 through 10, indicate that SSDOS-II comes much closer to predicting experimental data than SSDOS. Comparison of both model version predictions to actual measured values is presented in Figure 6b. SSDOS-II tends to straddle the 45° line while SSDOS is consistently above the 45° line.

The discussion to date, although it has not been so stated, is only applicable to continuously cooling thermal cycles exhibiting very rapid heating times, relatively short cooling times, and low to intermediate maximum temperatures. The restriction to high heating rate comes from the exclusion of the possibility of nucleation beginning during the heating portion of the thermal cycle. The restriction to relatively short cooling times comes from the fact that excessive carbide precipitation depletes the matrix in carbon and, therefore, changes the equilibrium carbide/matrix minimum chromium concentration. Note that matrix carbide depletion is not expected to occur in welding due to the relatively rapid thermal cycle seen in practical weldment HAZs.

The restriction to low and intermediate temperatures comes from the experimentally observed fact that sensitization development induced at a constant cooling rate increases up to a given critical temperature (range) and then precipitously drops, Figure 11. It should be emphasized that this drop takes place even though the material

heated above this critical temperature undergoes exactly the same cooling time/temperature thermal cycle once it reaches the critical temperature as the material only heated up to the critical temperature. Previous work, Figure 12, indicates that a distinct change in kinetics occurs upon heating SS above a given critical temperature.[14]

This problem was addressed in SSDOS by assuming a change in kinetics once the material went above a critical temperature (approximately 1000°C, depending on material carbon composition); kinetics were changed by a decrease in effective chromium diffusivity.[2,4] This change in diffusivity was empirically determined base on limited continuous cooling data. Both the change in kinetics and estimation of the appropriate temperature to initiate the change in kinetics are approached differently in SSDOS-II. The temperature needed to be reached to initiate kinetics change is assumed to be related to the carbon solid solubility temperature based on reported solubility expressions, as illustrated in Figure 11a.[15] This treatment assumes that carbon atoms precipitated at, or segregated to, grain boundaries at temperature below the solid solubility temperature reduce nucleation times over "clean" grain boundaries heated into the solid solubility region.

The exact effective grain boundary dissolution temperature is probably greater than the equilibrium solubility temperature and will be a function of heating rate. However, as the present experimental data is insufficient to quantitatively assess this phenomenon, the model simply assumes the kinetic change takes place when the material is heated above the solid solubility temperature. These equations are input into the model as a function temperature and alloy composition.

The nucleation kinetics changes in SSDOS-II for material heated below and above the solid solubility temperature are based on changes in nucleation time; the effective diffusivity of chromium is assumed to remain unchanged. The SSDOS-II predictions of nucleation time as influenced by maximum temperature is illustrated in Figure 13. The quantitative kinetic changes used in SSDOS-II were developed using data best fit techniques; the resultant agreement with experimental data can be seen in Figures 6 through 10.

Model Application To Weld HAZ

The characteristics of weld thermal histories important to sensitization development are generally thought of as being the maximum temperature reached during heating and the average cooling rate during cooling. The authors propose that this is too simplified a view of sensitization development, and that, in fact, very little sensitization development occurs if one runs weld simulation cycles based on maximum temperature and average cooling rate. It appears that maximum sensitization development occurs in the portion of weld thermal cycle near the maximum temperature, on both the heating and cooling side, where the rate of change of temperature is smallest. Outside this

region the material generally sees a relatively rapid rate of temperature change on heating and on cooling where sensitization development is relatively minimal.

An illustration of HAZ weld induced sensitization development during girth welding of a 356mm diameter, Schedule 160, 304 SS pipe is illustrated in Figure 14. The pass-by-pass, inside wall, thermal histories were experimentally measured while the chromium depletion width and EPR-DOS values were predicted using SSDOS. These predictions indicate that the majority of sensitization development, for this position with respect to the weld centerline, was associated with only two out of 16 passes, pass 6 and 7. The early passes exhibited fast heating and cooling rates as well as maximum temperatures that promoted carbide dissolution and high chromium minimums, while the latter passes didn't reach high enough temperatures to promote carbide growth.

Pass 6 had a maximum temperature near 1000°C which promoted high grain boundary chromium minimums and a decrease in chromium depletion in the region near maximum temperature. Limited increase in the size of the depleted zone took place during the relatively slow cooling cycle. The majority of the development occurred in the temperature region exhibiting a slow rate of temperature change in pass 7, i.e., near maximum temperature during heating as well as cooling. These observations demonstrate the need for "correct" simulation of the complete weld thermal cycle and the unacceptability of weld simulation using only maximum temperature and (average) cooling rate.

Another weld simulation problem that arises is the need for inclusion of deformation effects. The presence of plastic strain has been shown to accelerate both isothermal and continuous cooling induced sensitization development.[2-6] Dynamic strain measurement techniques used to monitor HAZ deformation indicates that cyclic plastic strain above and beyond that simply induced by thermal expansion is present in the HAZ.[4,16]

Deformation measuring devices, Figure 15, were placed on the inside surface of SS girth welds in order to monitor weld induced deformation. Results for twelve out of 35 passes of deformation parallel to, and 0.5 cm from the weld centerline, for a 610mm diameter, 25.4mm wall, high carbon, Type 304 SS the girth weld, Figure 16, indicate a consistent pattern of deformation takes place during welding.[4,16] A proposed graphical analysis of the deformation taking place for a given pass is presented in Figure 17.[3,15] Note that the removal of thermally induced strains, based on the measured thermal history corresponding to the center of deforming region, still leaves strain components, called "mechanical" strain, several times the magnitude of the thermal strain, Figure 17a.

An analysis of mechanical strain, Figure 17b, indicates that initial plastic strain is compressive, followed by a region of tensile plastic strain and then a second region of compressive plastic strain. This is then followed by a tail-off region that determines final residual (compressive or tensile) elastic strain. A detailed discussion of this analysis is

given elsewhere.[16] Addition of the absolute values of strain for the three major regions results in an effective strain term on a pass-by-pass basis, as illustrated in Figure 18.

As demonstrated above, realistic weld thermal histories, including the shape of the temperature/time history instead of a simple estimate of maximum temperature and cooling rate, is required for accurate predictions. The thermal history module currently used in the model is based on the weld thermal history prediction program developed by Solomon.[17] This thermal prediction methodology yields thermal histories as a function of weld heat inputs, pipe thickness and bead placement.

The basic continuous cooling model was modified to allow input of thermal histories using Solomon's weld thermal prediction scheme. Thermal histories for a 610mm diameter, 25.3mm wall, SS pipe are shown in Figure 19. Comparison of predicted thermal histories with experimentally determined histories yielded reasonable agreement with actual maximum temperatures, Table 2. Weld heat input and bead positions for this weld simulation calculation were taken from an actual weldment and are exhibited in Figure 20.[4]

Assessment of sensitization development under multipass conditions and the effect of carbon content and strain on sensitization development in high carbon Type 304 and 316 SSs is presented in Figure 21. Three sets of sensitization development values, calculated using the thermal histories presented in Figure 21, are plotted as a function of strain level and carbon content for each type of SS. The first set of sensitization values assumes only thermal effects with no strain component. This is assumed to be the minimum sensitization derived from the weldment. The second set assumes base thermal effects accelerated by the measured mechanical strain induced on a pass by pass basis, Figure 18. The third set assumes thermal effects accelerated by the cumulative measured strain induced on a pass by pass basis. Use of the pass by pass measured strain assumes complete strain recovery during each weld pass. Use of the cumulative measured strain assumes no strain recovery during each weld pass. One assumes the "correct" strain values lie between the two latter extremes.

Sensitization development is found to dramatically increase with increasing carbon content and strain for both alloys. Little EPR-DOS differences are found between the alloy types at low carbon concentration, with Type 316 tending to be more resistant to sensitization development at high carbon contents. The Type 304 alloy composition is that of the pipe material previously girth welded: 0.058C, 18.67Cr, 8.78Ni, 0.16Mo, and 0.059N (wt%). The post-weld EPR-DOS value found using the field cell EPR-DOS measurement technique was 28, which agrees reasonably well with the predicted EPR-DOS.[4]

Weld heat affected zones from all but the low carbon (0.02 w%) welds would be expected to exhibit substantial reduction of area when subjected to CRT testing in

simulated BWR coolant water as illustrated in Figure 1. Use of the generally accepted rule of thumb that material exhibiting between 2 to 5 EPR-DOS is susceptible to IGSCC in BWR reactor environments also indicates that only the low carbon alloys would not be susceptible to IGSCC in the as-welded conditions in BWRs not using supplemental IGSCC mitigation techniques. More quantitative predictions of IGSCC are possible by combining the EPR-DOS predictions of the SSDOS model with the model of Ford[18] which predicts crack growth rates as a function of EPR-DOS.

Conclusions

A computer-based model has been developed that is capable of predicting continuous cooling induced sensitization, with and without the presence of prior strain. Modeling of sensitization development kinetics required the use of nucleation time as a function of specimen temperature. Modeling of the experimentally observed decrease in sensitization development kinetics once temperatures over the solid solubility temperature of carbon was reached required a decrease in nucleation kinetics. Application of continuous cooling sensitization modeling to welding situation proved feasible.

References

1. E.C. Bain, R.H. Aborn and J.J.B. Rutherford, Trans. Amer. Soc. Steel Treating, 21, 481 (1933).

2. S.M. Bruemmer, "Quantitative Measurement and Modeling of Sensitization Development in Stainless Steels," DOE-NE-37963-7, Oregon Graduate Center, Beaverton, OR 97006 November, (1988).

3. S.M. Bruemmer, "Quantitative Modeling of Sensitization Development in Austenitic Stainless Steel," Corrosion Journal, **146**(9), 698, 1990.

4. D.G. Atteridge, S.M. Bruemmer, "Evaluation of Welded and Repair Welded Stainless Steel for LWR Service," U.S. Nuclear Regulatory Commission Report: NUREG/CR-3613, Vol. 3, No. 2, (1986).

5. J.W. Simmons, "Effects of Prior Deformation Continuous Cooling of Type 316 Austenitic Stainless Steel," Edited by D.G. Atteridge, Oregon Graduate Institute of Science and Technology, Beaverton, OR 97006-1999, U.S. Nuclear Regulatory Commission Report: NUREG/GR-003, August (1991).

6. A.H. Advani, "Deformation Effects on the Development of Grain Boundary Chromium Depletion (Sensitization) in Type 316 Austenitic Stainless Steels," DOE-NE-37963-12, July (1990).

7. D.G. Atteridge, S.M. Bruemmer, R.E. Page, "Evaluation and Acceptance of Welded and Repair-Welded Stainless Steel for LWR Service," U.S. Nuclear Regulatory Commission Report: NUREG/CR-3613, (1983).

8. D.G. Atteridge, S.M. Bruemmer, L.A. Charlot, R.E. Page, "Evaluation of Welded and Repair-Welded Stainless Steel for LWR Service," U.S. Nuclear Regulatory Commission Report: NUREG/CR-3613, Vol. 3, No. 1 (1985).

9. F.P. Ford, D.F. Taylor, P.L. Anderson, and R.G. Ballinger, EPRI Report, NP50648, Feb, 1987.

10. W.L. Clarke, R.L. Cowan and W.L. Walker, in ASTM STP 656, 99 (1978).

11. W.L. Clarke, General Electric Report GEAP-21382, U.S. Nuclear Regulatory Commission NUREG-0251-1 (1976).

12. S.M. Bruemmer, L.A. Charlot, D.G. Atteridge, "Compositional Effects in the Sensitization of Austenitic Stainless Steels," U.S. Nuclear Regulatory Commission Report: NUREG/CR-3618 (1984).

13. J.W. Simmons, D.G. Atteridge, L.E. Murr, S.M. Bruemmer, "Effects of Prior Deformation on the Sensitization of Type 316 Austenitic Stainless Steel II: Continuous Cooling Sensitization," Recent Trends in Welding Science and Technology, Edited by S.A. David and J.M. Vitek, International Conference Proceedings, pp. 321-5, (1990).

14. H. Ikawa, Y. Nakao, and K. Nishimoto, "Study of Weld Decay in SUS 304 Precipitation Phenomena of $M_{23}C_6$ During Thermal Cycles," Technical Reports of Osaka University, No. 1434 p. 369, (1978).

15. M. Deighton, J. Iron Steel Inst., p. 1012, November (1970).

16. D.G. Atteridge, W.E. Anderson, "Cyclic Work Hardening Induced in the Heat Affected Zone During Multi-Pass Welding," presented at the International Conference on Welding and Performance of Pipelines, London, England, November (1986).

17. H.D. Solomon, S. Levy, "HAZ Temperatures and Cooling Rates as Determined by a Simple Computer Program," Trends in Welding Research in the United States, pp. 173-206, Edited by S.A. David, Conference Proceedings, (1982).

18. S.M. Bruemmer and L.A. Charlot, Sensitization Development in Austenitic SS: Comparison Between STEM-EDS and EPR Measurements, Corrosion Journal,44(6), 328, 1988.

Acknowledgements

This work was supported by the Division of Engineering Technology, Office of Nuclear Regulatory Research of the U.S. Nuclear Regulatory Commission. Additional support was also received from the Advanced Nuclear Reactor Technology Office and U.S. Department of Energy.

TABLE 1. Thermomechanical Processing for Continuously Cooled Type 316 SS Specimens

Prior Strains, %	Heating Rate, °C/sec	Maximum Temperature, °C	Cooling Rates, °C/sec
0, 5, 10, 20	50	800	0.05, 0.10, 1.0[1]
0, 5, 10, 20	50	850	0.05, 0.10, 1.0[1]
0, 5, 10, 20	50	900	0.05, 0.10, 1.0
0, 5, 10, 20	50	950	0.05, 0.10, 1.0
0, 5, 10, 20	50	1000	0.05, 0.10, 1.0
0, 5, 10, 20	50	1050	0.05, 0.10, 1.0

[1]0% prior strain specimens not subjected to this treatment.

TABLE 2. Comparison of Measured and Predicted Maximum Temperatures on a Pass-by-Pass Basis

	Peak Temperature, °C	
Pass Number	Measured	Predicted
1	940	946
2	759	756
3	899	902
4	742	737
5	725	723
6	517	578

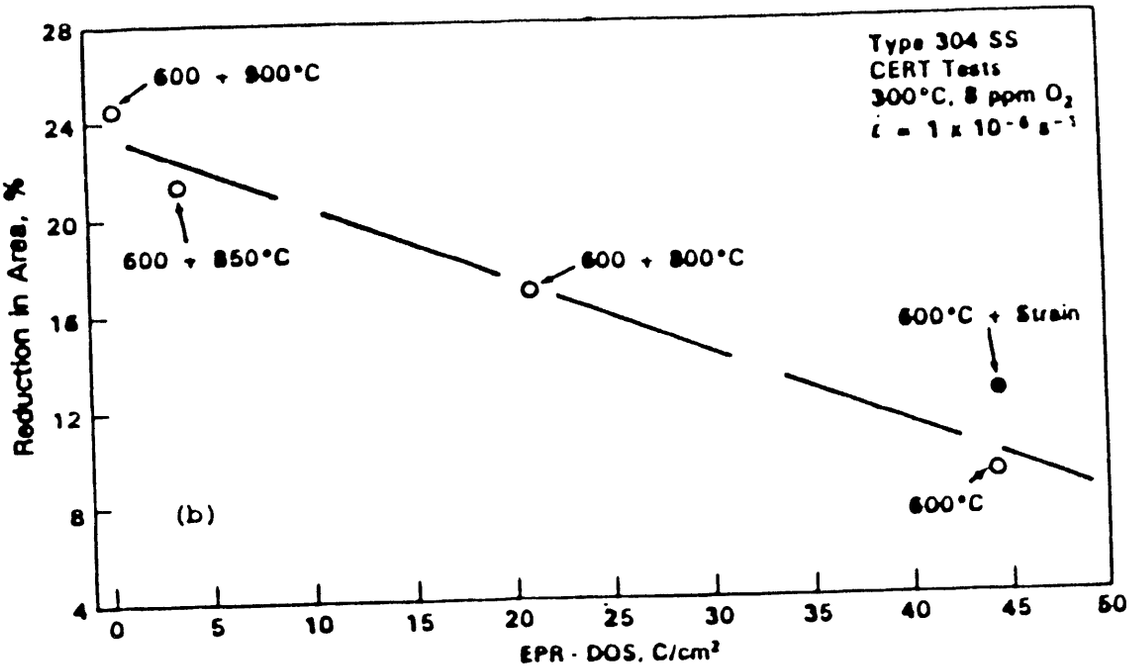

FIGURE 1. Correlation Between Degree of Sensitization as Measured by EPR and Ductility as Measure in Slow-Strain-Rate Stress Corrosion Cracking Tests

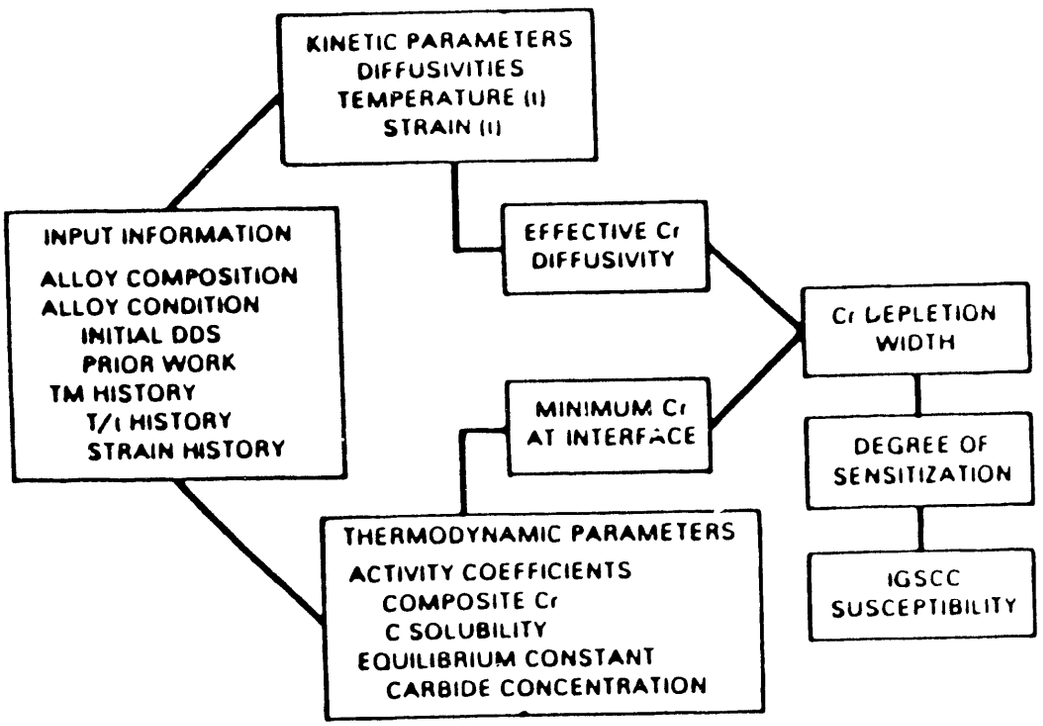

FIGURE 2. Flow Diagram Illustrating Degree of Sensitization Prediction Approach

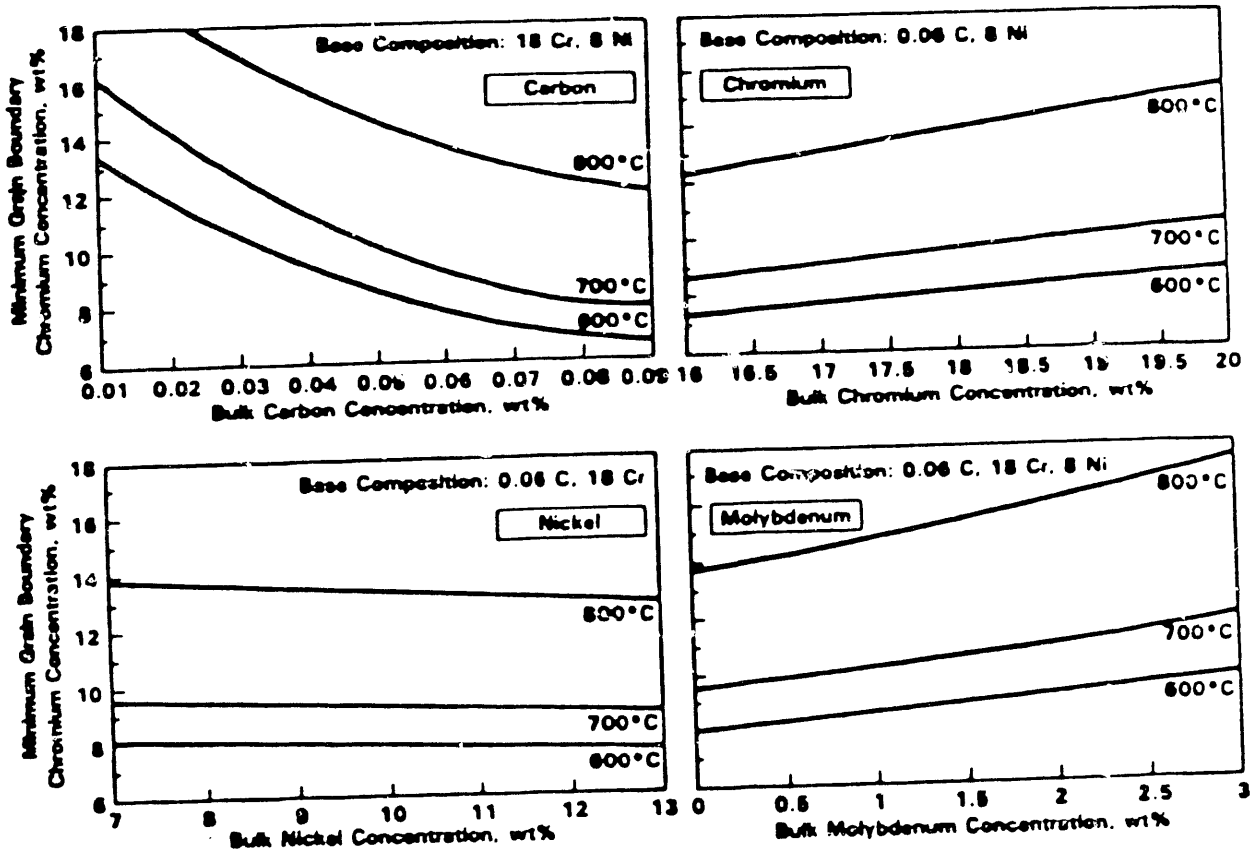

FIGURE 3. Model Predictions Illustrating Bulk Composition Effects on Sensitization

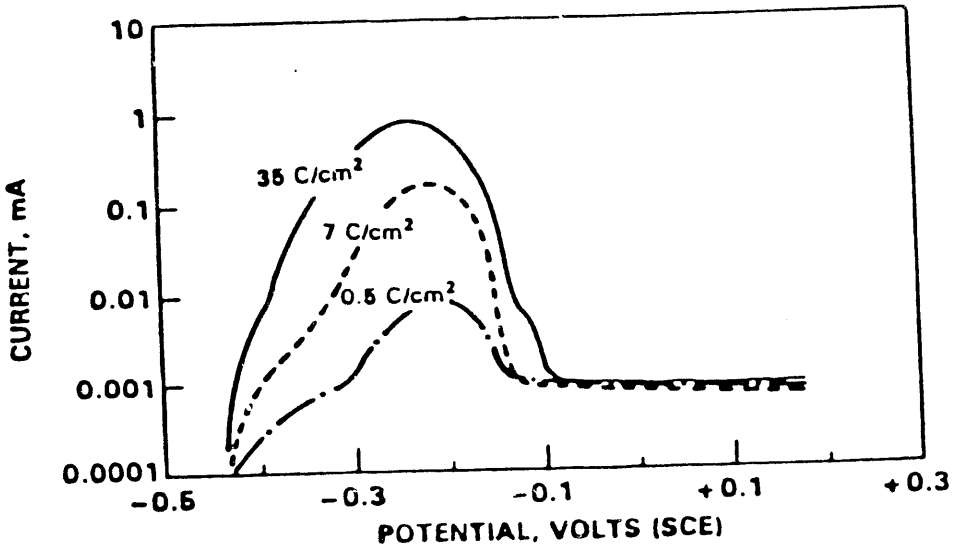

FIGURE 4. Examples of Potentiokinetic Reactivation measurements for Different Levels of Sensitization, EPR-DOS Values are Indicated

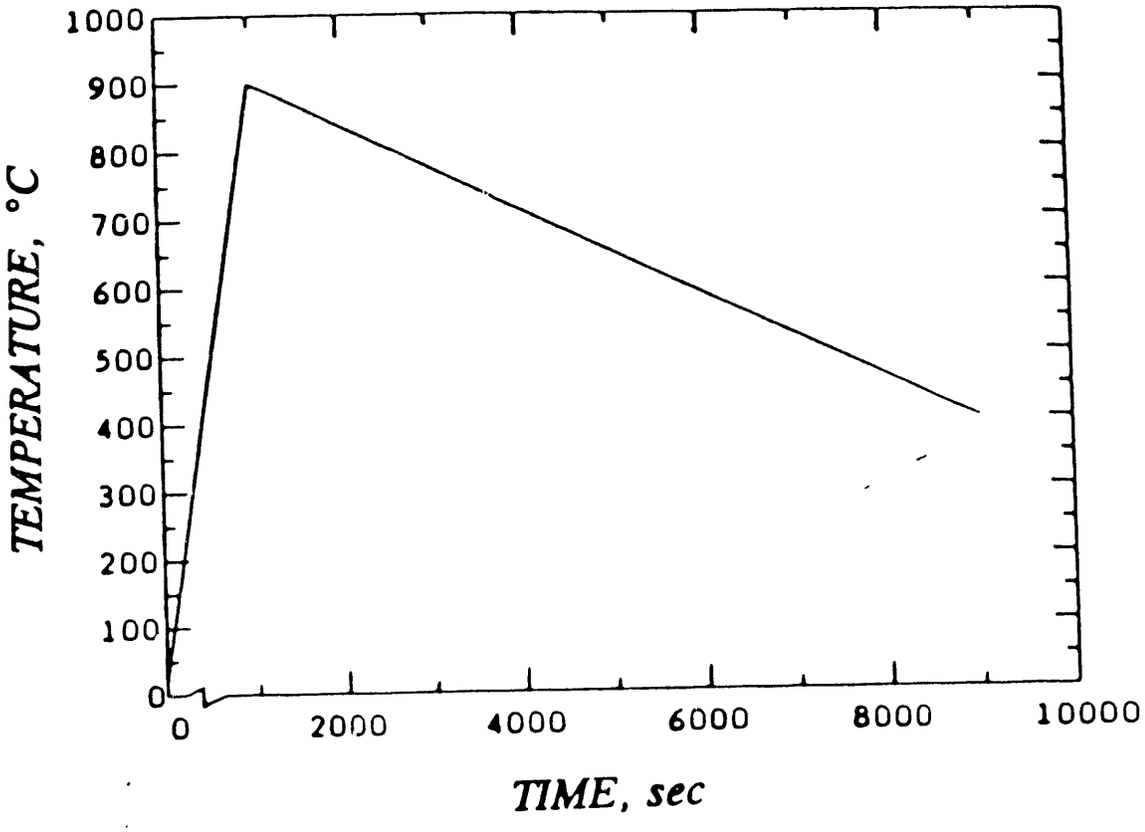

FIGURE 5. Typical Continuous Cooling Gleeble Thermal Cycle Illustrating Maximum Temperature and Linear Cooling Rate

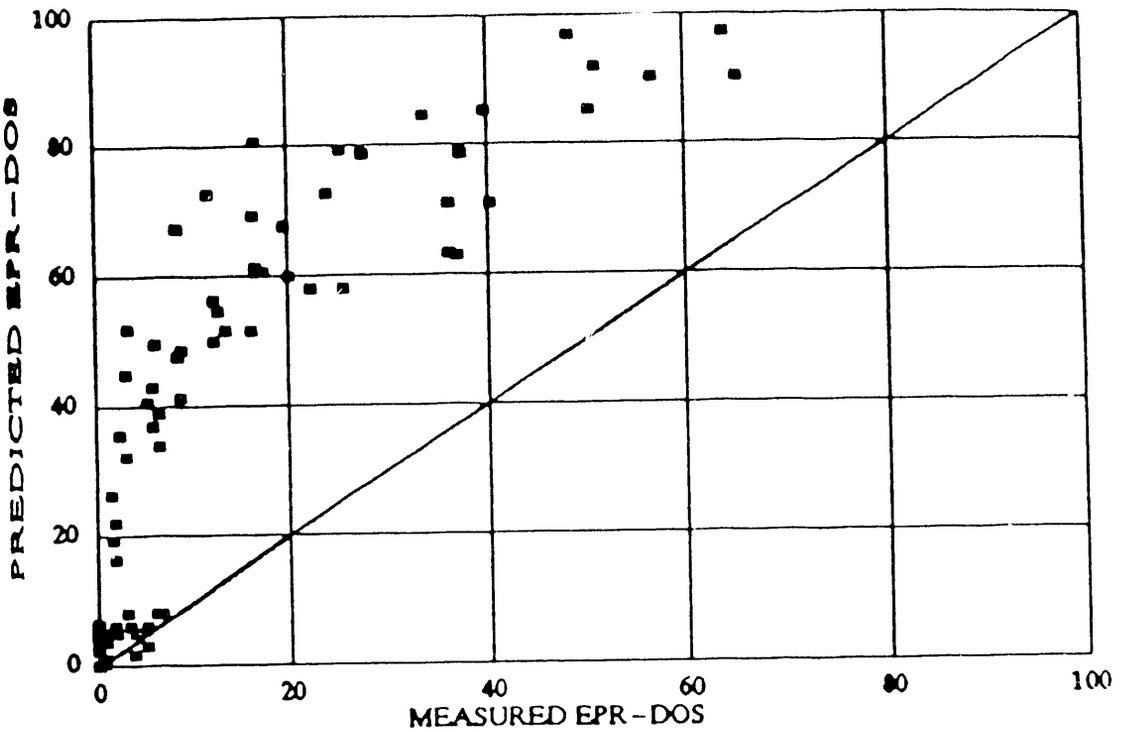

(a)

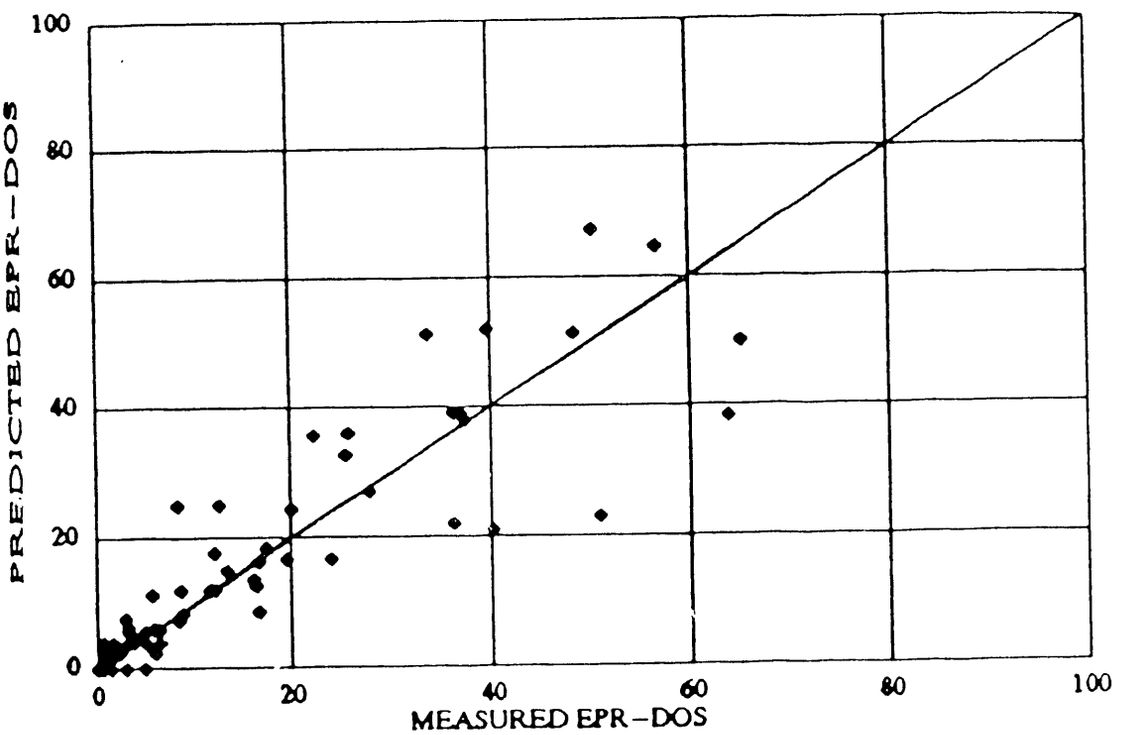

(b)

FIGURE 6. Comparisons between measured and Predicted EPR-DOS for Continuous Cooling Results from Mill Annealed and Prestrained Specimens: a) SSDOS; b) SSDOS-II

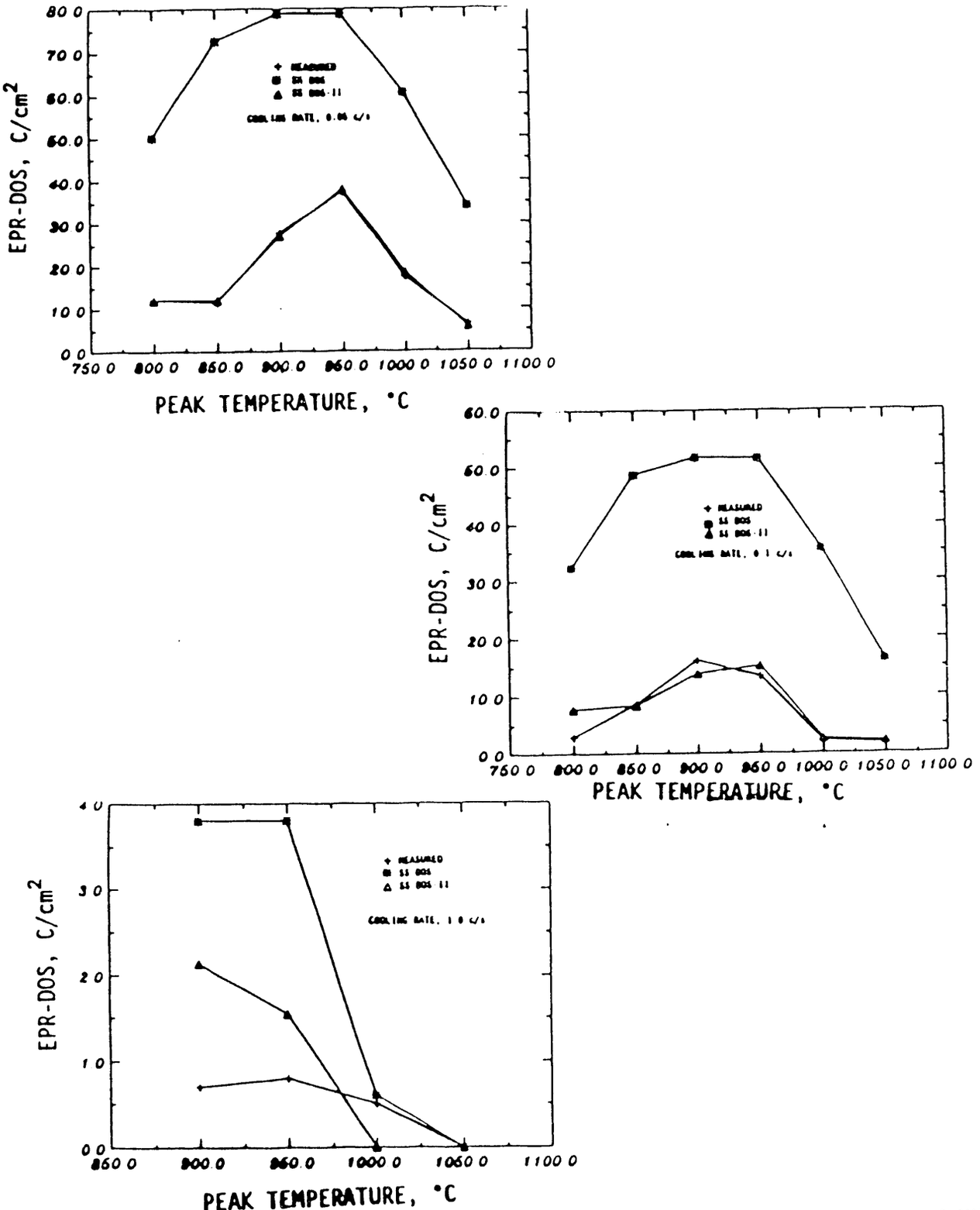

FIGURE 7. Comparison Between Measured and Predicted EPR-DOS Values for Mill Annealed Material as a Function of Peak Temperature and Cooling Rate

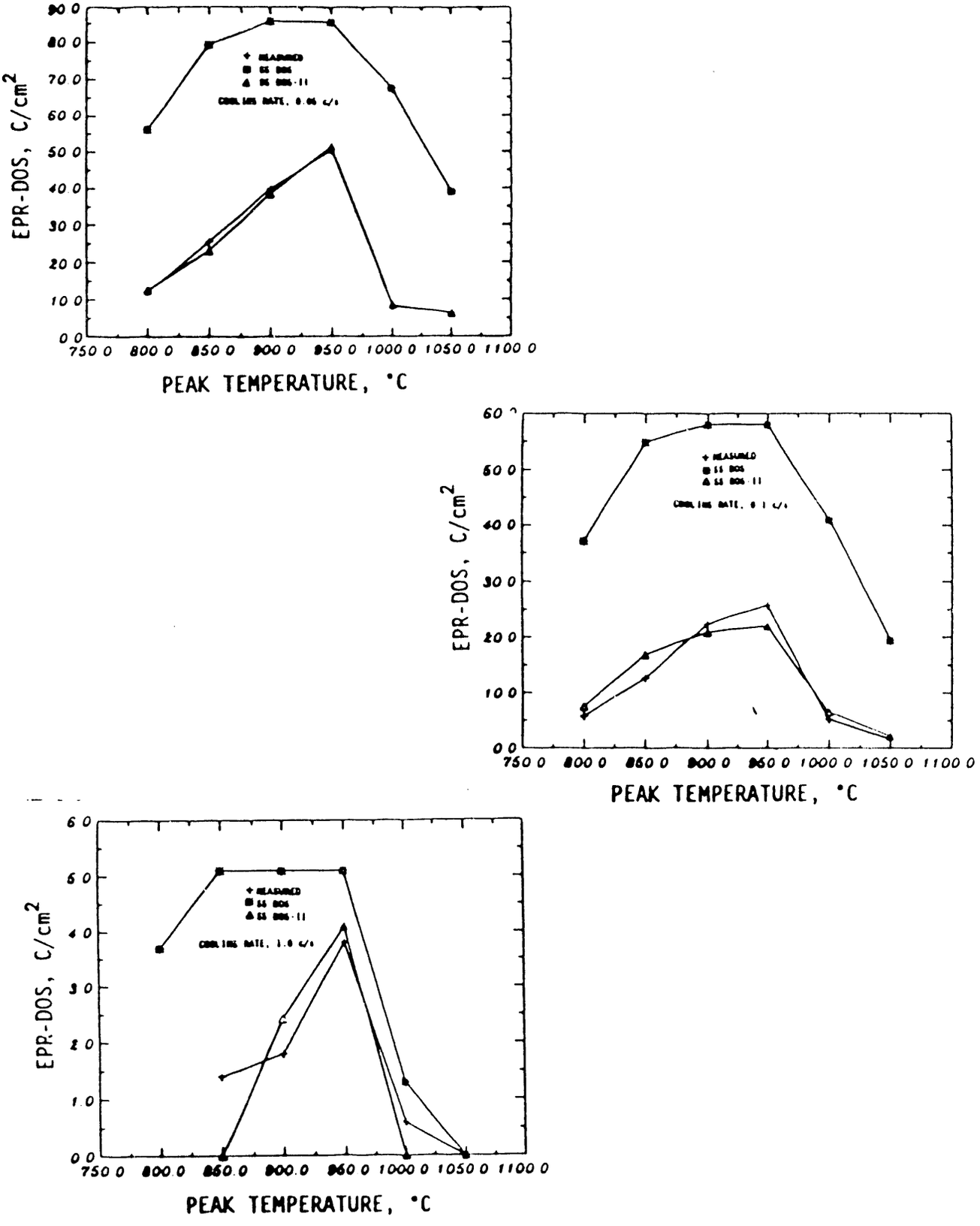

FIGURE 8. Comparison Between Measured and Predicted EPR-DOS Values for Mill Snnealed Material Prestrained 5% as a Function of Peak Temperature and Cooling Rate

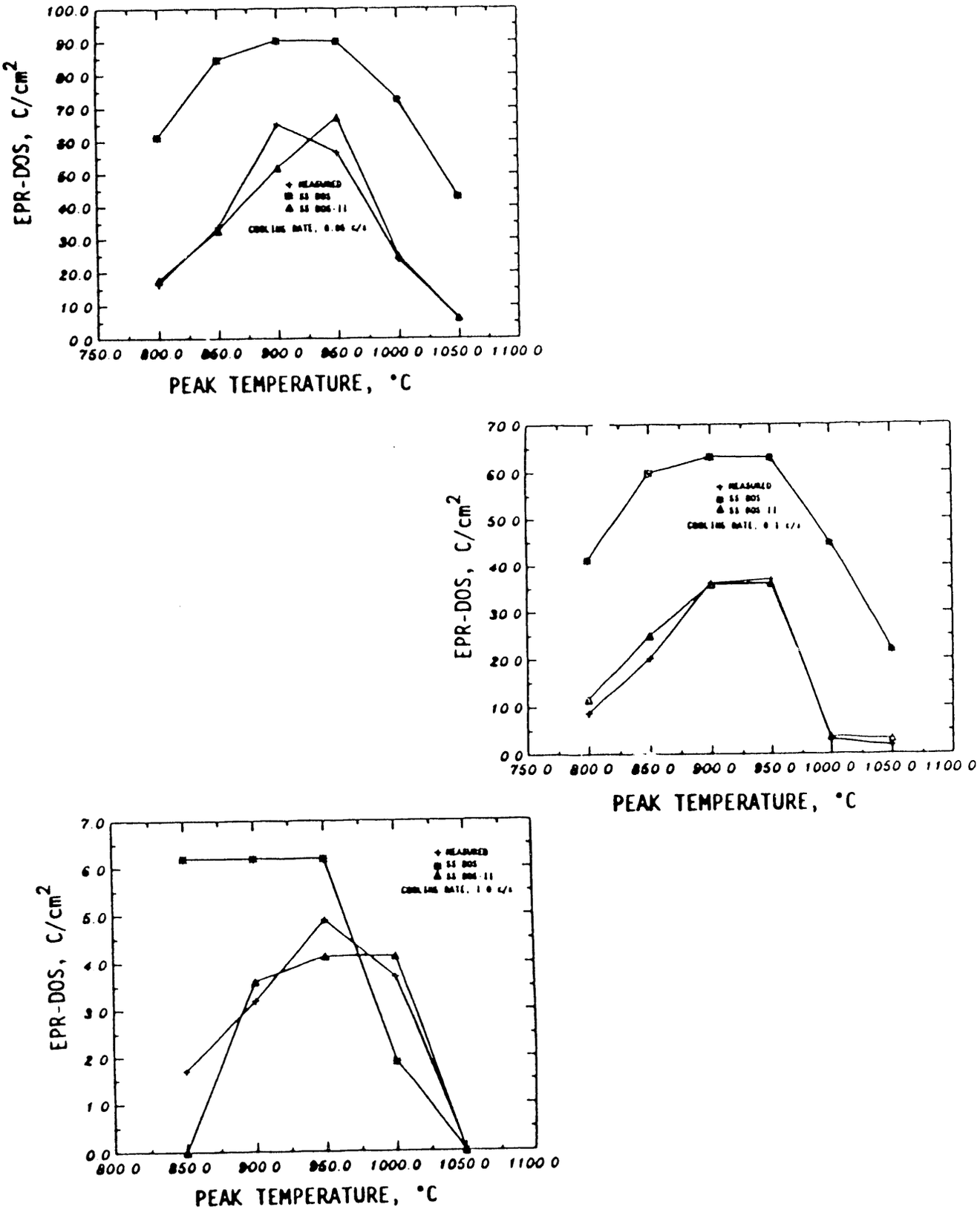

FIGURE 9. Comparison Between Measured and Predicted EPR-DOS Values for Mill Annealed Material Prestrained 10% as a Function of Peak Temperature and Cooling Rate

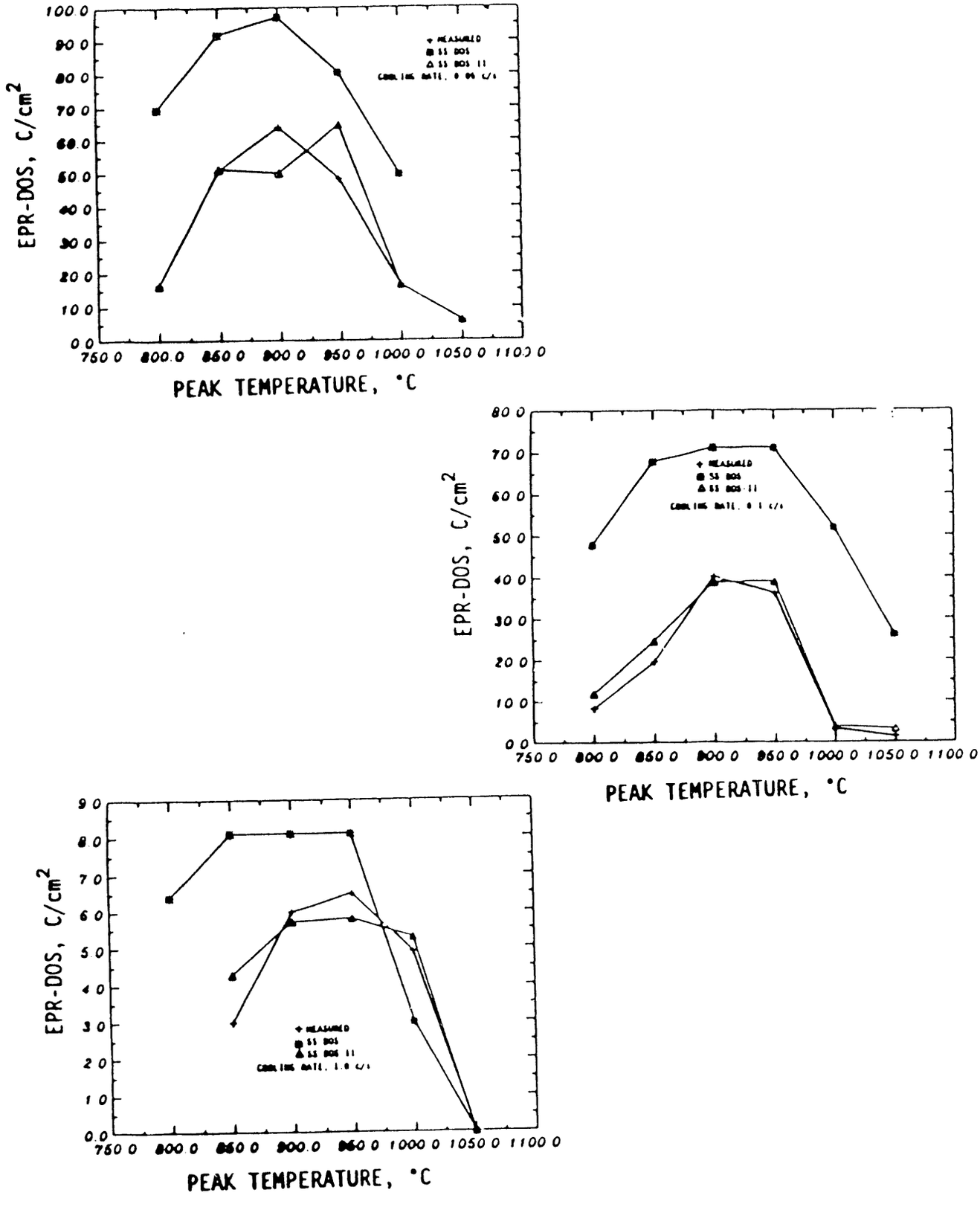

FIGURE 10. Comparison Between Measured and Predicted EPR-DOS Values for Mill Annealed Material Prestrained 20% as a Function of Peak Temperature and Cooling Rate

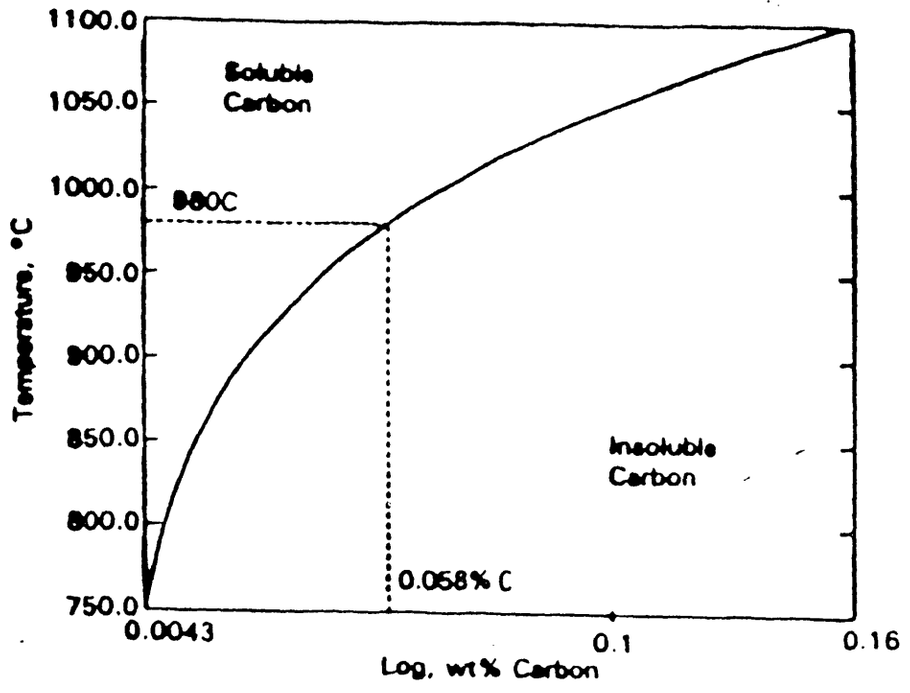

(a)

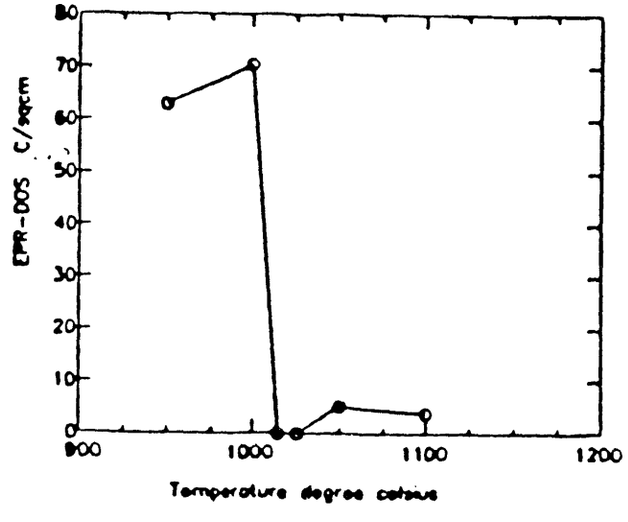

(b)

FIGURE 11. Variation of Carbon Solubility for Type 316 Stainless Steel as a Function of Temperature and Carbon Content (a), and Change in Sensitization Induced by Continuous Cooling as a Function of Maximum Temperature(b)

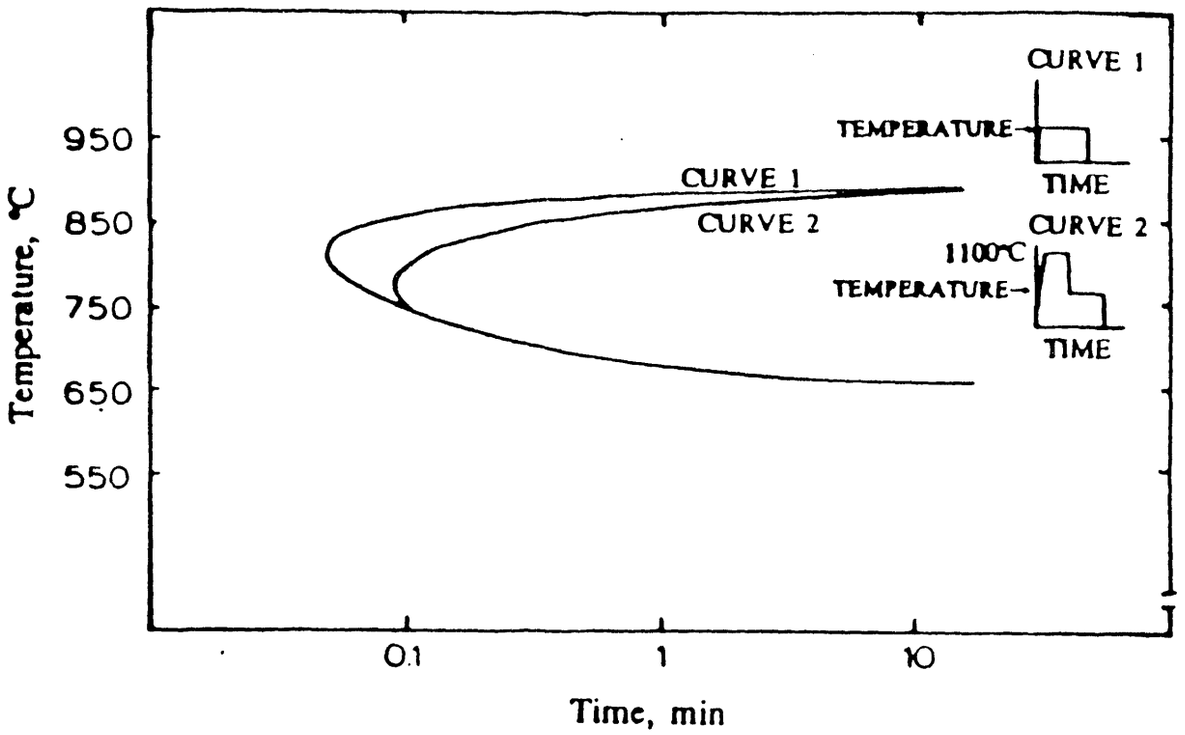

FIGURE 12. Change of $M_{23}C_6$ Precipitation Kinetics due to Pre-Isothermal Hold Temperature for a 0.05% Type 304 (After Ikawa et al.[22])

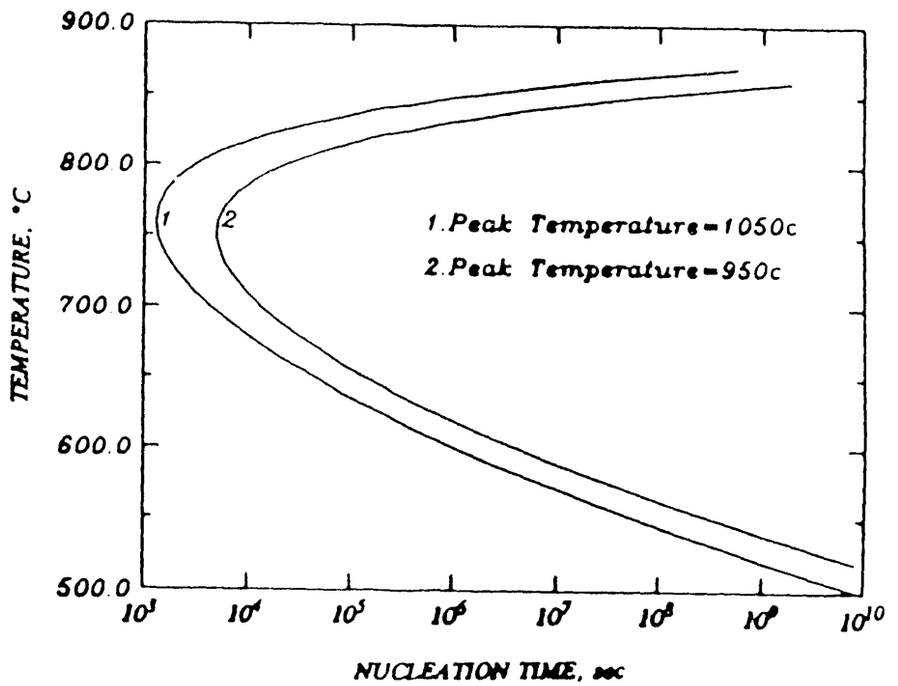

FIGURE 13. Change in Predicted Nucleation Time as Function of Continuous Cooling Cycle Peak Temperature

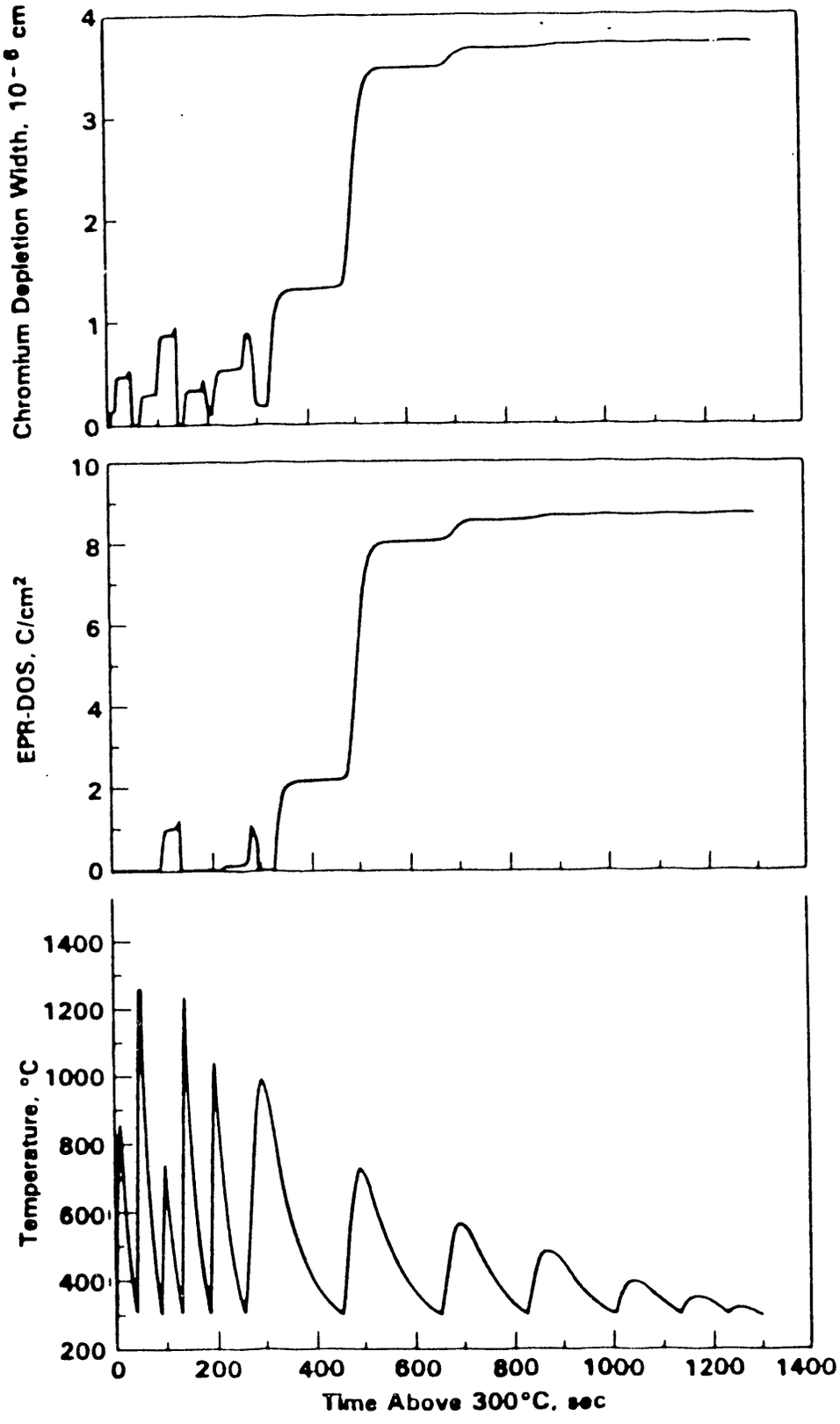

FIGURE 14. Development of the Degree of Sensitization 4mm from the Weld Centerline in a 356mm Diameter Schedule 160 SS Pipe Weld

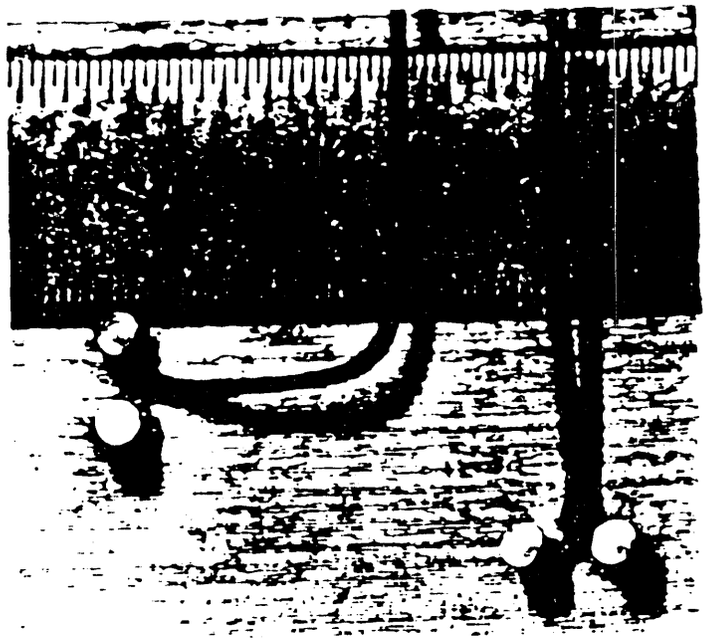

(a)

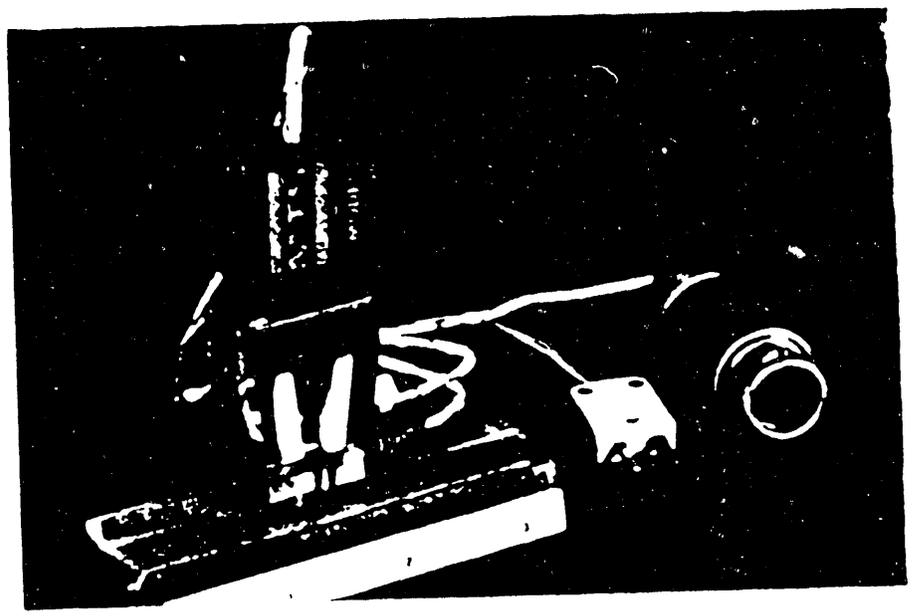

(b)

FIGURE 15. Surface Movement Monitoring clip Gage Attachment Studs (a) and Completely Assembled Gage (b)

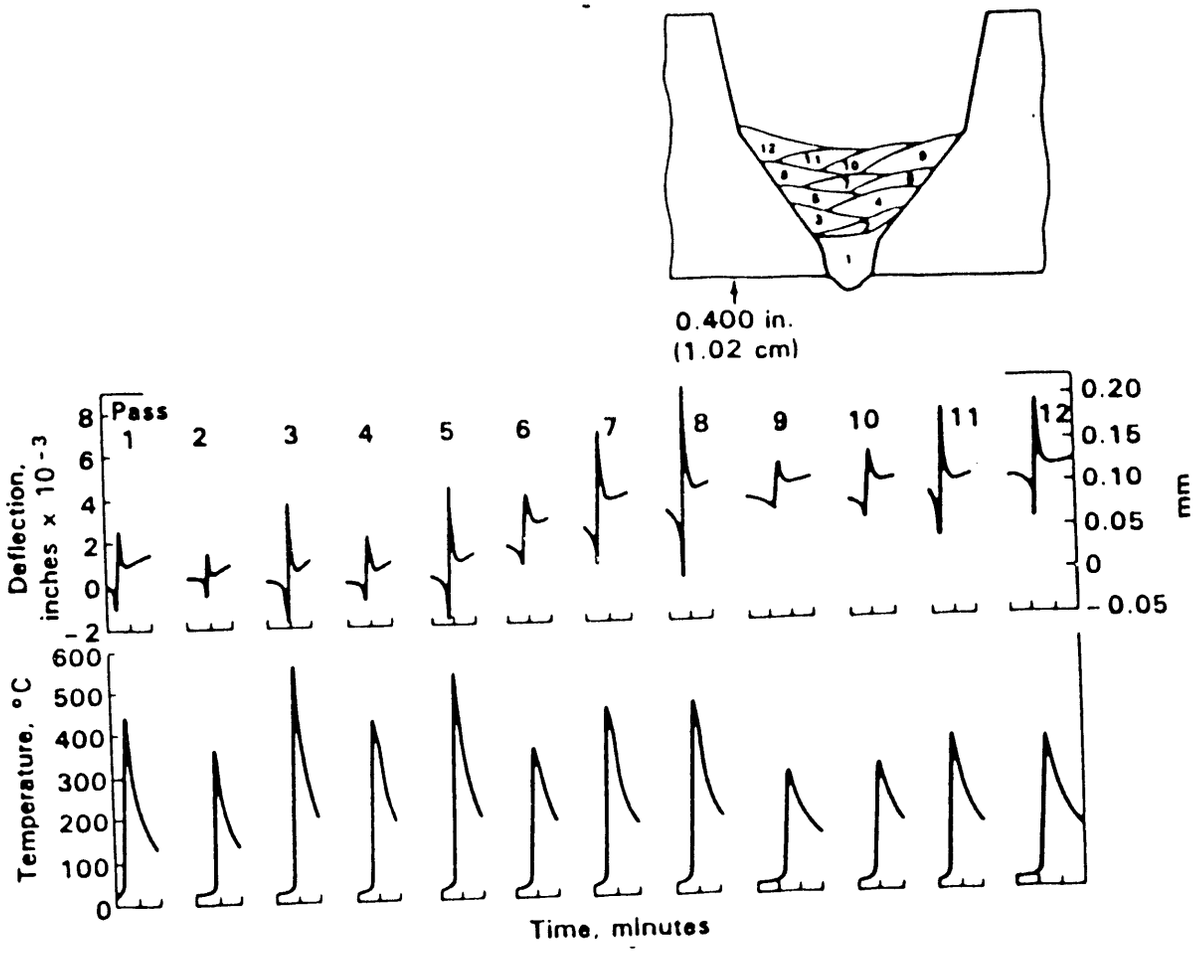

FIGURE 16. Temperature and Surface Deflection Parallel to the Weld Centerline Surface 10mm from the Weld Centerline for the First Twelve Passes of a 610mm Diameter Pipe Weld

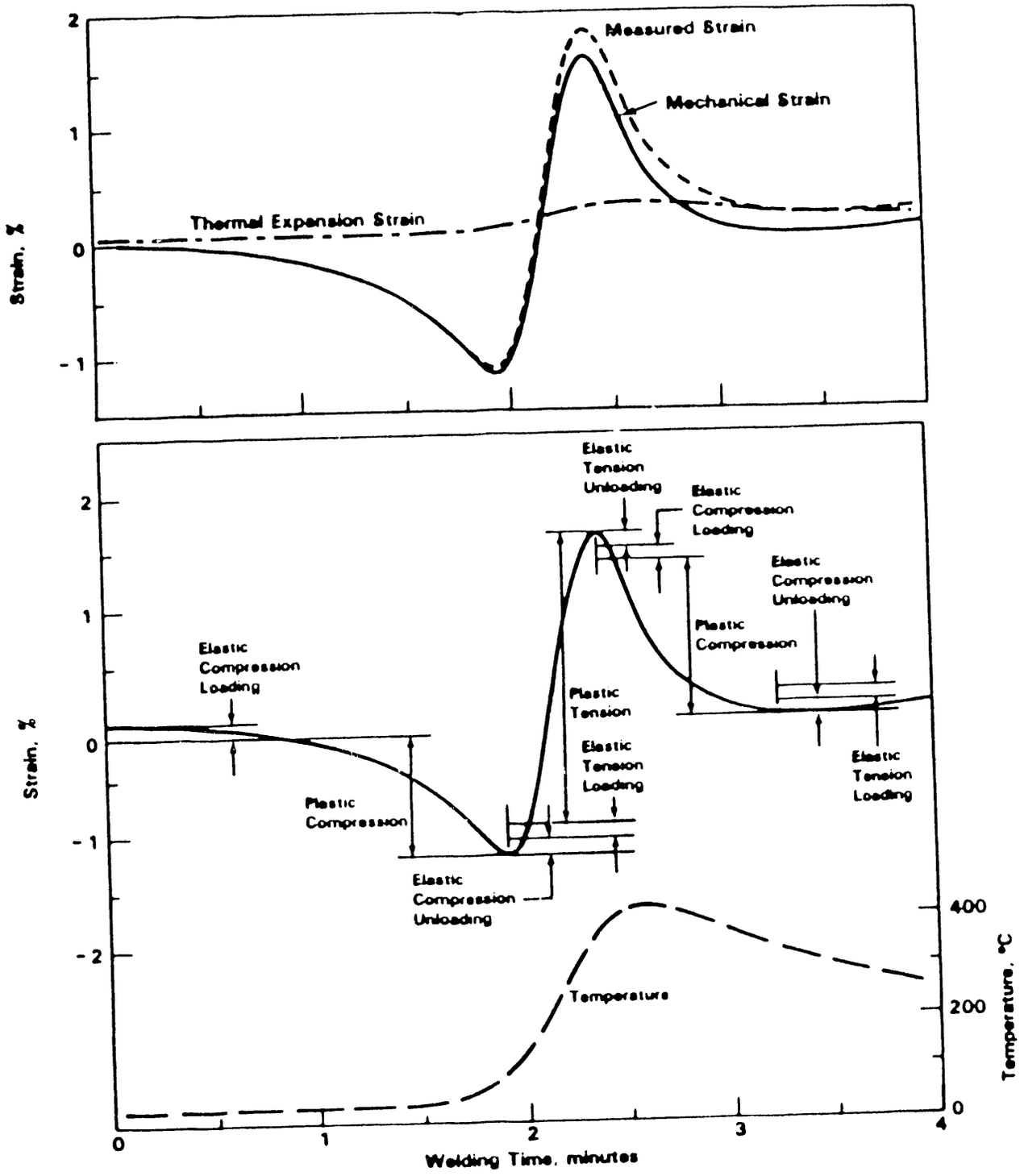

FIGURE 17. Thermal and Mechanical Stain Components of Stains Measured Parallel to the Weld Centerline. Data for pass 18 at the weld centerline

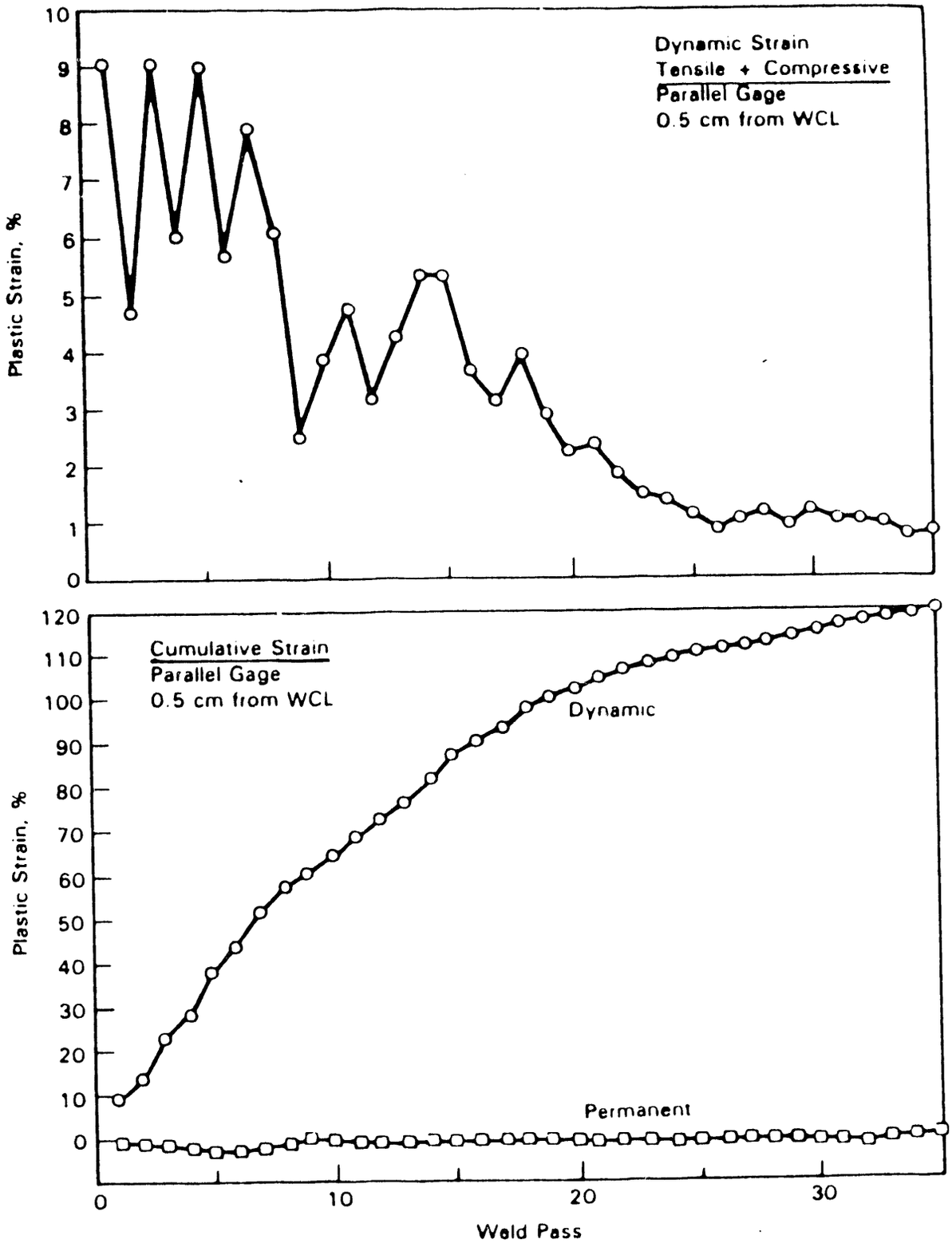

FIGURE 18. Pass-by-Pass and Cumulative Dynamic Stain compared to the Permanent Plastic Strain Induced at the Inner Surface 0.5mm from the Weld Centerline

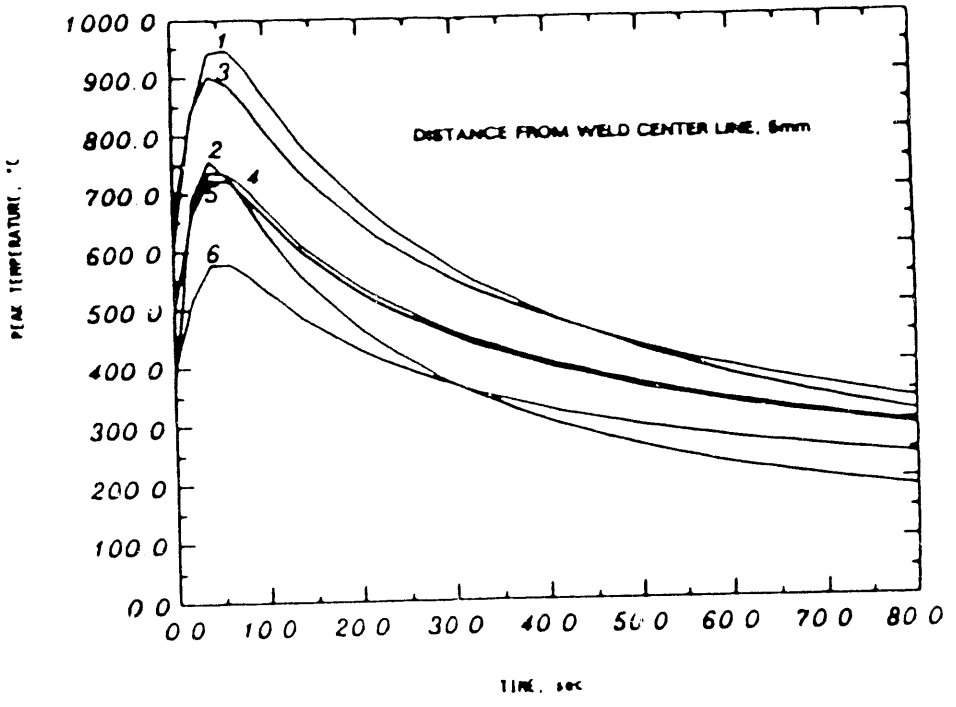

FIGURE 19. Predicted HAZ Girth Weld Thermal Histories 5mm from Weld Centerline on the Inside Surface of a 610mm Diameter 25.4mm Wall, Type 300, Series SS Pipe as a Function of Pass

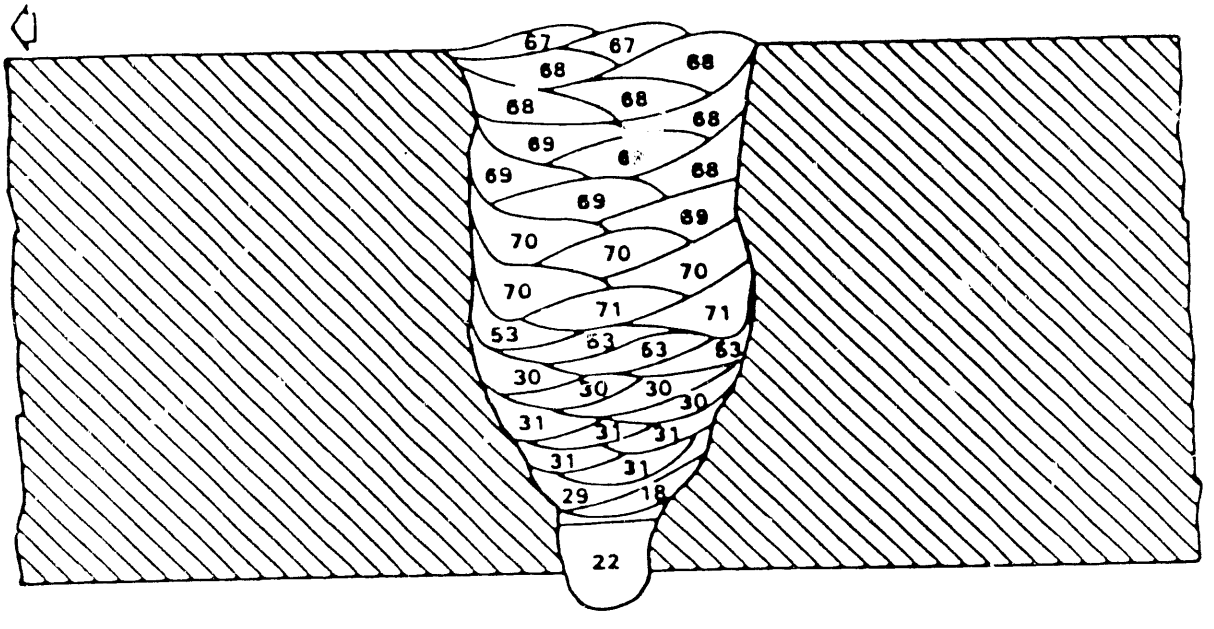

FIGURE 20. Schematic Illustration of Weld Bead Position and Welding Heat Input (kJ/in.) used to Girth Weld a 610mm Diameter, 25.4mm wall, Type 304 SS Pipe

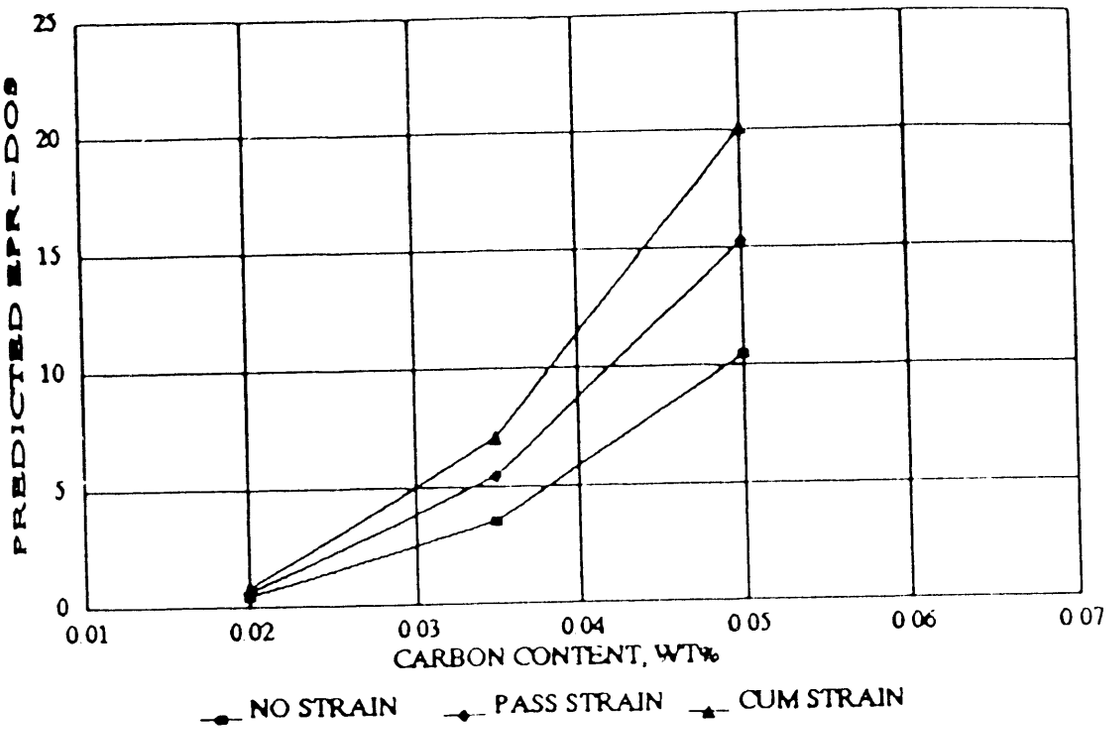

(a)

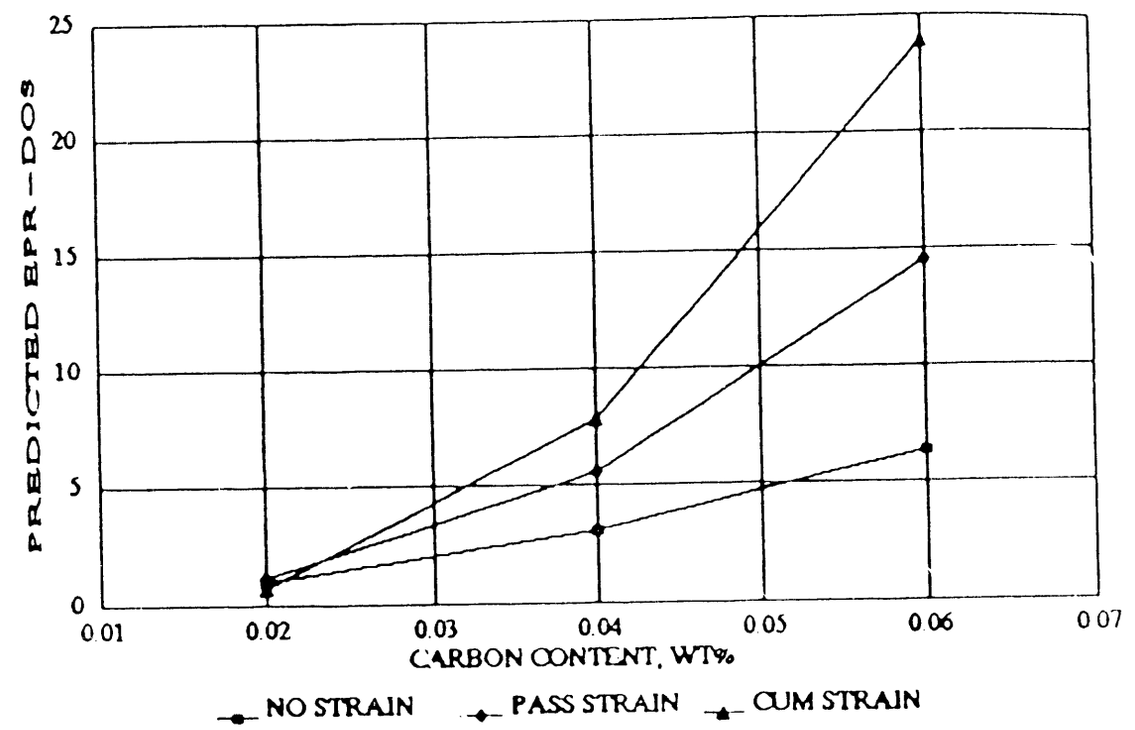

(b)

FIGURE 21. Predicted Post-Weld EPR-DOS 5mm from the Weld Centerline on the Inside Surface of a 610mm Diameter pipe as a function of alloy composition and local strain: (a) Type 304; (b) Type 316

END

DATE
FILMED
2/03/92